ENGINEERING

Extreme nonlinearity by layered materials through inverse design

Zhi Zhao[1]†, Rahul Dev Kundu[1]†, Ole Sigmund[2], Xiaojia Shelly Zhang[1,3,4]*

Biological materials such as seashell nacre exhibit extreme mechanical properties due to their multilayered microstructures. Collaborative interaction among these layers achieves performance beyond the capacity of a single layer. Inspired by these multilayer biological systems, we architect materials with free-form layered microstructures to program multistage snap-buckling and plateau responses—accomplishments challenging with single-layer materials. The developed inverse design paradigm simultaneously optimizes local microstructures within layers and their interconnections, enabling intricate layer interactions. Each layer plays a synergistic role in collectively achieving high-precision control over the desired extreme nonlinear responses. Through high-fidelity simulations, hybrid fabrication, and tailored experiments, we demonstrate complex responses fundamental to various functionalities, including energy dissipation and wearable devices. We orchestrate multisnapping phenomena from complex interactions between heterogeneous local architectures to encode and store information within architected materials, unlocking data encryption possibilities. These layered architected materials offer transformative advancements across diverse fields, including vibration control, wearables, and information encryption.

INTRODUCTION

Architected materials with nonlinear mechanical responses hold great potential for a wide range of applications (*1*). For example, components designed for impact protection require materials that exhibit force plateau regimes over a long deformation range to effectively absorb energy and mitigate high impact force (*2*, *3*). Wearable devices such as tremor suppression need materials capable of repeatedly dissipating energy while complying with large deformations of soft biological tissues (*4*). In addition, data storage and encoding within architected materials demand diverse deformation modes and wide design flexibility (*5*). Customizing these unique nonlinear mechanical responses of architected materials to meet specific application requirements is crucial to fully harness their potential. Hence, much attention has been devoted to the design and realization of these architected materials for versatile functionalities, including energy dissipation (*6*–*8*), energy absorption (*3*, *9*), information encoding (*5*, *10*), and wearables (*11*–*13*). State-of-the-art studies (*3*, *6*, *14*–*16*) have successfully programmed and prototyped nonlinear stress-strain relations in planar architected materials with a single design layer. However, some extreme nonlinear responses, such as multistage snap buckling and plateau responses, may not be realizable within a single in-plane layer, which could limit the achievable programmability and functionality of architected materials.

Biological materials in nature often reveal intricate microstructures with multiple layers, for example, seashell nacre (*17*, *18*) illustrated in Fig. 1A. Collaborative interaction among these multiple layers often leads to performance that surpasses the capacity of a single layer. Prior studies have used architected multilayer materials to enable deformation and stiffness controls, such as auxetic deformation (*19*, *20*), area preservation (*21*), spatiotemporal shape evolution (*22*), and ultrastiff mechanical performance (*23*). Here, we harness the bioinspired concept of layered microstructures to architect materials that achieve extreme nonlinear responses, such as multistage snap buckling and multistage plateau responses. The achievement of these extreme nonlinear responses stems from the synergistic interactions among different soft material layers, which is challenging, if at all possible, to achieve by a single material layer alone.

To inversely design the architected materials for nonlinear target responses, existing studies have used topology optimization (*6*, *24*, *25*) and machine learning (*15*, *26*–*28*) as design approaches. Topology optimization stands out as an effective generative method (*29*, *30*) for the free-form design of materials and structures, given its ability to explore the entire geometric design space to achieve the target responses. In this work, we develop an inverse design framework to simultaneously optimize the local microstructure within each layer and architect their interconnections, enabling complex and collaborative layer interactions within these architected materials. The proposed framework presents several advantages over existing inverse design methodologies for nonlinear stress-strain responses. The framework optimizes nacre-like multiple layers along with their interconnections in a continuum setup, which significantly expands the design space compared to similar work involving a single-layer setup (*3*, *31*) or lattice structures (*32*). At the same time, it bypasses the immense computational expense of a full 3D design problem with a hybrid finite element method using both 2D and 3D elements. The proposed multilayer design setup allows precise control of challenging nonlinear responses, such as multistage plateau and snap-buckling including bistability, while bypassing the challenges of single-layer design setup, such as internal contact (see the Supplementary Materials for a comparison study). Furthermore, it uses a gradient-based topology optimization scheme that explores a larger design space compared to intuitive and parametric solutions (*33*) and offers less overall computational time compared to machine learning–based methods (*27*, *32*, *34*) that generally involves a computationally intensive dataset generation and training phase (*35*).

We conduct high-fidelity simulations, use hybrid fabrication techniques, and perform experimental testing to demonstrate the inverse design and physical realization of layered architected materials, which

[1]Department of Civil and Environmental Engineering, University of Illinois Urbana-Champaign, Urbana, IL 61801, USA. [2]Department of Civil and Mechanical Engineering, Technical University of Denmark, Koppels Allé, Building 404, 2800 Kongens Lyngby, Denmark. [3]Department of Mechanical Science and Engineering, University of Illinois Urbana-Champaign, Urbana, IL 61801, USA. [4]National Center for Supercomputing Applications, Urbana, IL 61801, USA.
*Corresponding author. Email: zhangxs@illinois.edu
†These authors contributed equally to this work.

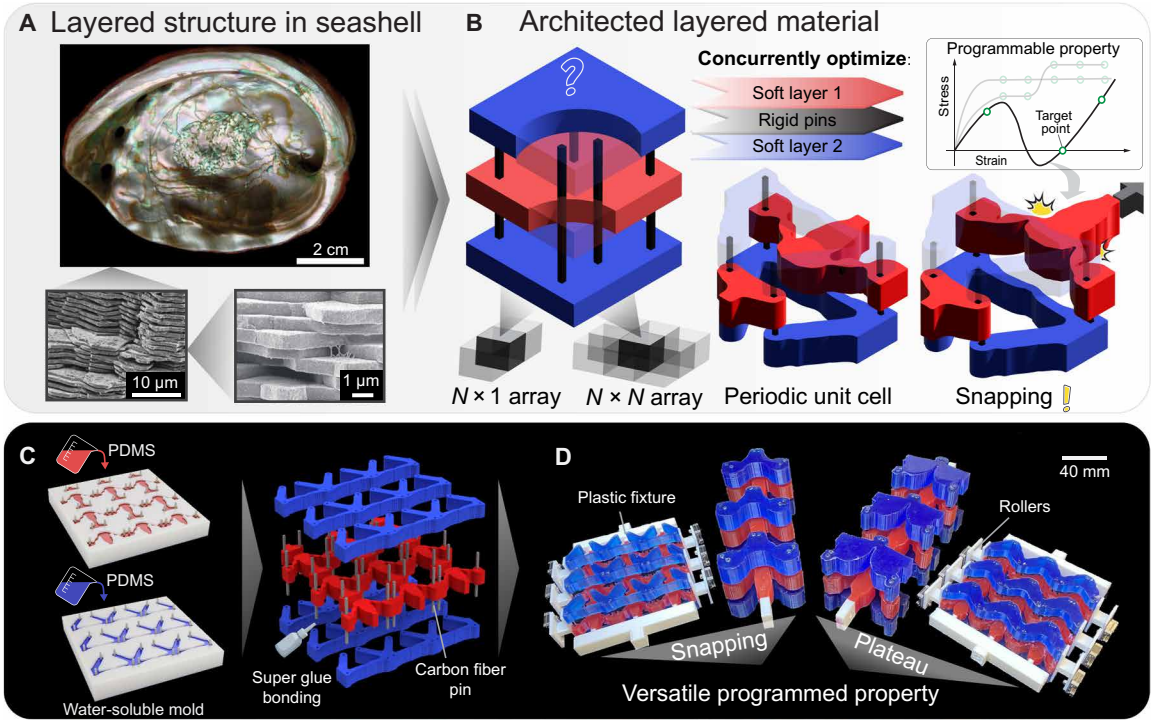

Fig. 1. Inverse design of layered nonlinear architected materials. (**A**) Images of layered structures found in seashell nacre (*17*, *18*). (**B**) Design of layered nonlinear architected materials with snapping properties. (**C**) Overview of the fabrication approach. (**D**) Collection of prototypes with versatile programmed properties. See movie S1 for the inverse design process, fabrication, and experimental validation. Photo credits: (A) 2 cm scale photo, courtesy of J. Varner, adapted from (*18*) with permission from Springer Nature, licensed under CC BY 4.0 (https://creativecommons.org/licenses/by/4.0/); 10 μM and 1 μM scale photos, adapted from (*17*) with permission from the Royal Society of Chemistry (https://doi.org/10.1039/9781849735315-00113).

successfully enable the function-oriented nonlinear responses. We explore the versatile potential of snap-buckling responses in layered architected materials, which have evolved from critical mechanical instabilities to valuable mechanisms for advanced applications. Snap-buckling materials dissipate energy efficiently during deformation, transitioning between stable states while maintaining resilience through repeated cycles (as demonstrated in Figs. 2A and 3C). These properties make them ideal for damping systems, such as vibration isolators, and biomedical wearable devices, such as tremor mitigation systems (*4*, *36*). Their tunable, adaptive behavior can also be utilized in soft wearables, such as joint-specific and patient-specific support (*37*), with structures offering controlled stiffness and tactile sensing (see a demonstrative example in Fig. 2F).

In addition, we investigate the programmable single- and multistage plateau responses enabled by layered architected materials, which can transfer external energy into stored energy (as illustrated in Fig. 4A). This feature benefits wearable devices and energy-absorbing systems, such as fall protection belts that reduce impact forces and car bumpers with multistage plateau responses that improve safety for both pedestrians and occupants by adapting to collision severity (*3*, *27*). In addition, our study uncovers a unique multisnapping response driven by the interplay of heterogeneous local layered architectures, enabling control over snapping sequences and the potential to encode and store information within soft materials (see a demonstrative example in Fig. 5). These findings highlight the potential of layered architected materials with programmable nonlinear responses for advancements in wearable devices, automotive safety systems, and information encryption.

RESULTS

The layered materials are constructed using periodic microstructural unit cells, each consisting of multiple soft elastomer layers. These layers are interconnected by rigid pins in the out-of-plane direction. In this study, we focus on square unit cells comprising three layers, as shown in Fig. 1B. The top and bottom layers share the same geometry because this sandwich configuration helps to mitigate unwanted out-of-plane deformations. The homogenized nonlinear properties of the layered material, characterized by effective stress and strain relations, can be determined by analyzing the mechanical responses of the layered unit cells with periodic boundary conditions under uniaxial loading (*14*). Depending on the various application-specific requirements, we can design the unit cells to exhibit periodicity either in one direction, forming an $N \times 1$ array, or in two directions, forming an $N \times N$ array.

Programming multistage snap buckling and plateaus in layered materials builds on the design of local microstructure (i.e., soft material distribution) within each layer and architectured interconnections (i.e., rigid pin distribution) among layers. As illustrated in Fig. 1B, the developed inverse-design framework concurrently optimizes the distributions of soft materials and rigid pins, which are parameterized by three sets of design variables. These variables are then used to characterize the mechanical responses defined by the

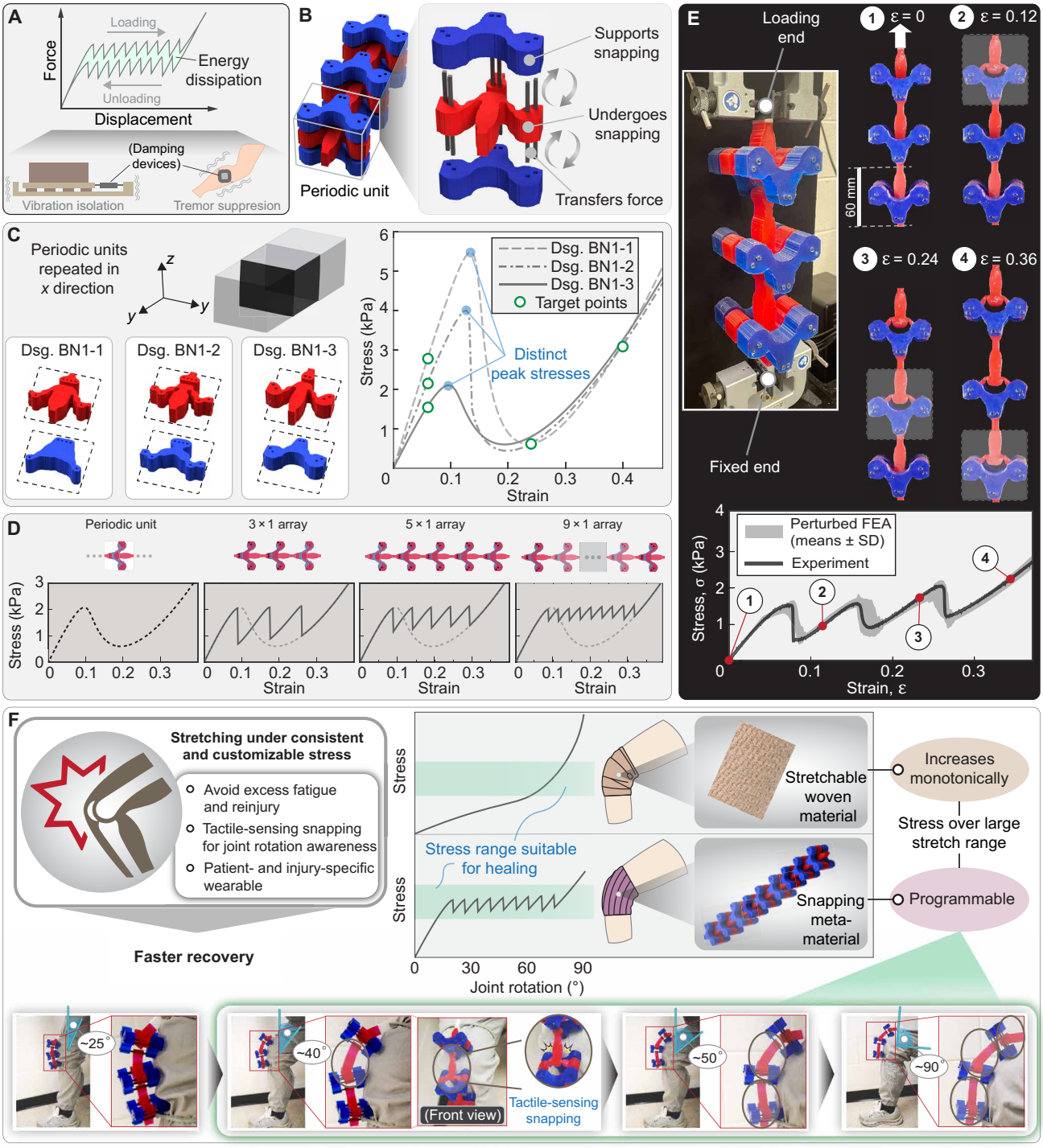

Fig. 2. Architected layered nonlinear material in $N \times 1$ array with snap buckling responses. (**A**) Illustration of energy dissipation capabilities and envisioned application scenarios. (**B**) A representative design example of the layered material. (**C**) A collection of designs (Dsg.) showcasing a range of initial stiffness and peak stress levels. (**D**) Numerical analysis showing the influence of varying unit cell numbers on the mechanical performance for design BN1-3. (**E**) Experimental validation for design BN1-3. See movie S3 for simulation and experimental validation. (**F**) Experimental demonstration of a soft wearable for injury recovery using design BN1-3.

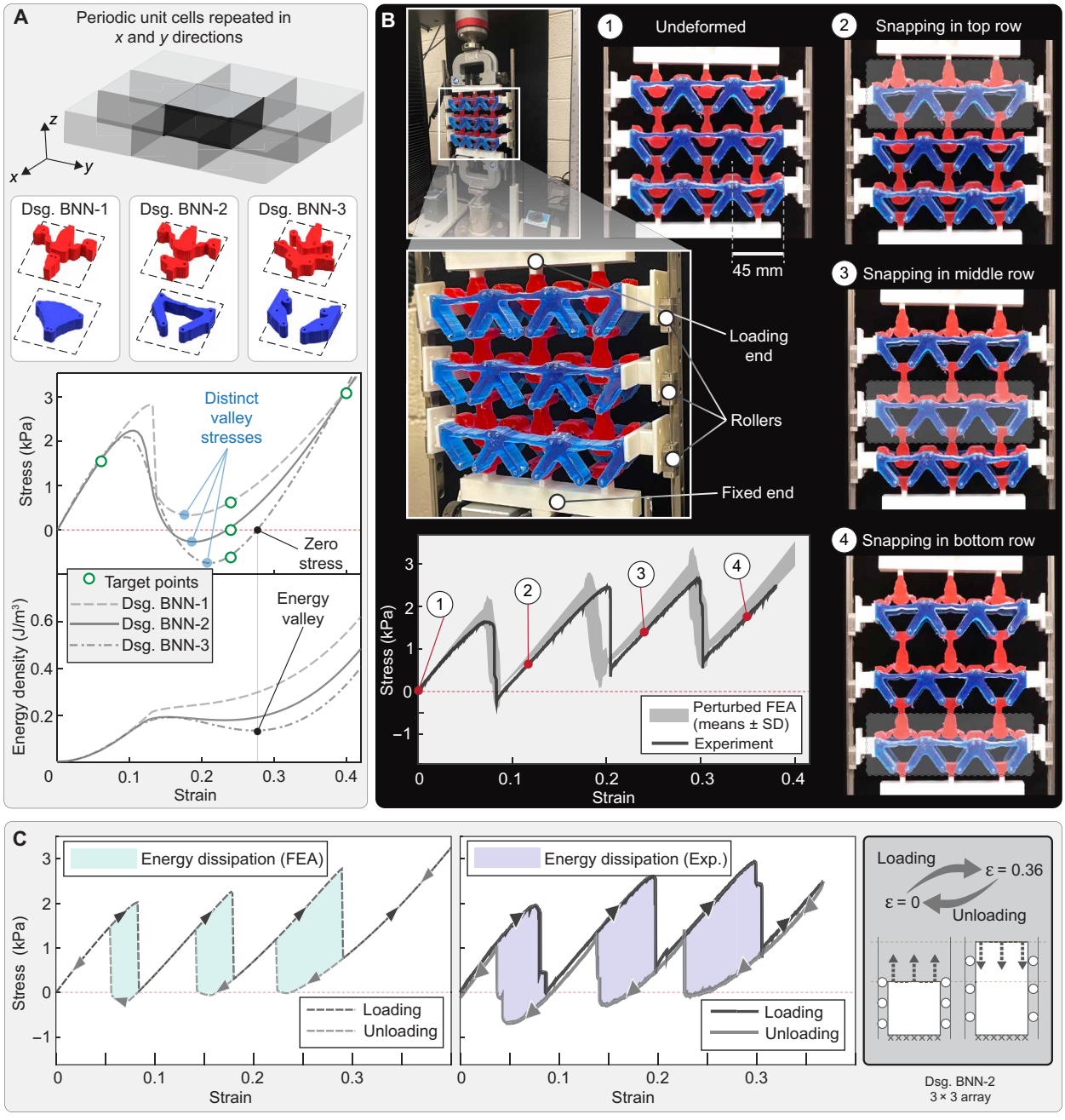

Fig. 3. Architected layered nonlinear material of $N \times N$ array with snap buckling responses. (**A**) The design setup and three designs with distinct valley stresses and energy profiles. (**B**) Experimental validation of the performance of design BNN-2. (**C**) Numerical simulation and experimental validation of a loading-unloading cycle demonstrating energy dissipation for design BNN-2. See movie S1 for simulation and experimental validation.

stored energy density functions through a tailored interpolation technique. With this design parameterization scheme, we formulate an inverse design problem: optimize the distributions of soft elastomers and rigid pins to minimize the discrepancy between the predicted stress-strain response via nonlinear finite element analysis (FEA) and the target nonlinear stress-strain relations. The optimization incorporates functional constraints to limit the excessive deformation and ensure well-defined geometry of each layer of the unit cell. We solve this constrained optimization problem using the method of moving asymptotes (*38*), a gradient-based optimizer based on analytically derived adjoint sensitivity analysis. The optimization framework enables the discovery of key interaction mechanisms among different layers that are crucial in achieving the target extreme nonlinear responses. For example, as illustrated in Fig. 1B, the top and bottom layers (here in blue), serving as supportive layers, sandwich and impose local restrictions on a middle layer (here in red) via rigid pins, thus triggering the snapping response of the middle layer. Leveraging the identified interaction mechanisms, we can

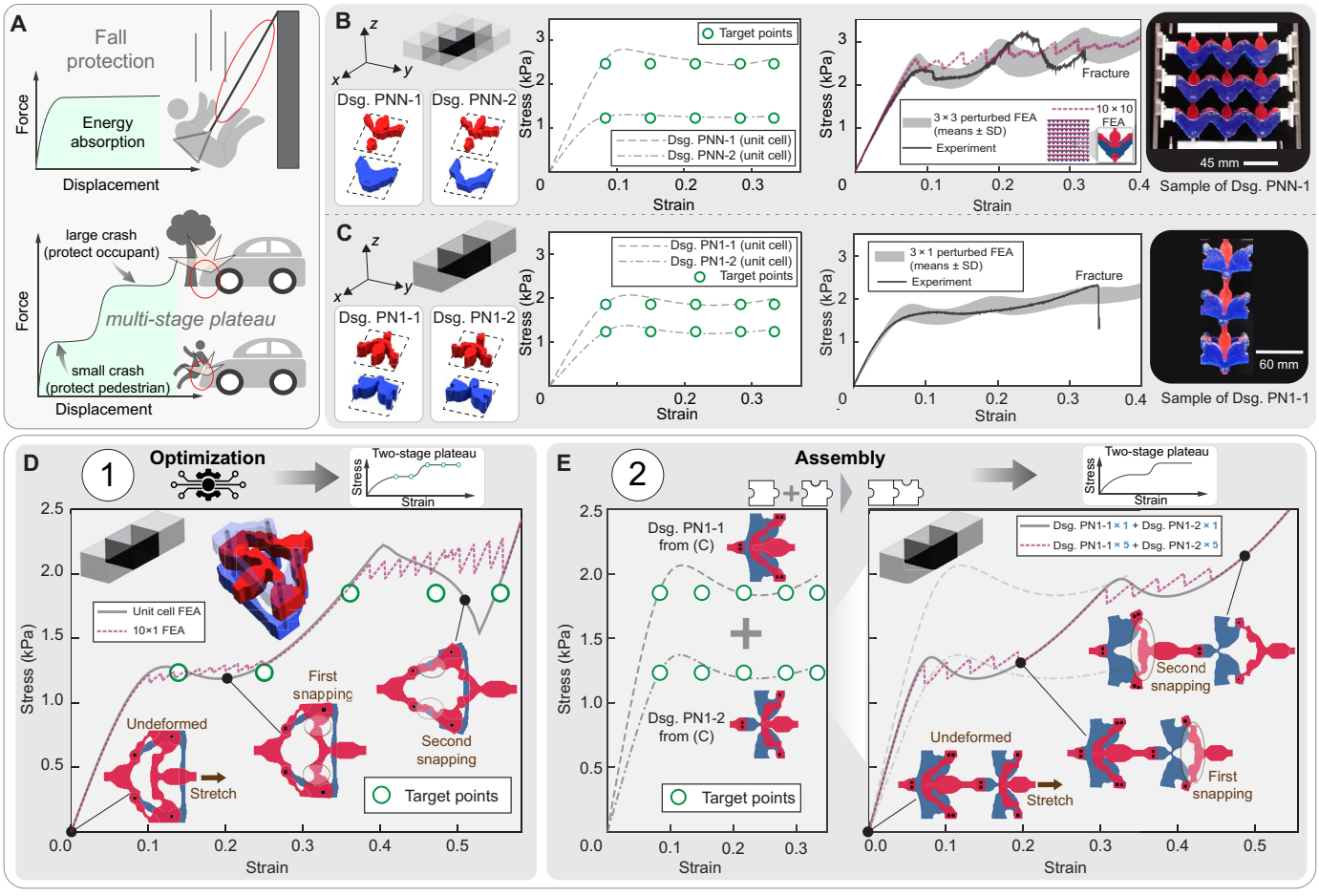

Fig. 4. Architected layered nonlinear material with single- and multistage plateau responses. (**A**) Illustration of energy absorption capabilities and envisioned application scenario. (**B**) Numerical designs and experiment for the designs with $N \times N$ array. (**C**) Numerical designs and experiment for the designs with $N \times 1$ array. (**D**) Approach 1 for achieving multistage plateau response through direct optimization of the unit cell. (**E**) Approach 2 for achieving multistage plateau response by assembling single-plateau unit cells. See movies S4 and S5 for simulation and experimental validation for design PN1-1 and PNN-1, respectively.

realize precise control over complex nonlinear responses in the periodic unit cells, such as snap buckling with distinct peak and valley stresses, and single and multiple plateau responses. Details of FEA and the inverse design framework are provided in the Supplementary Materials.

To physically realize and validate our inversely designed layered materials that exhibit a range of extreme nonlinear responses, we use a hybrid fabrication approach to prototype four representative designs, as illustrated in Fig. 1 (C and D). These samples are experimentally tested to validate the extreme nonlinear responses of multistage snap buckling and plateau responses. The fabrication process and experimental procedures are detailed in the Supplementary Materials.

Architecting snap buckling responses

In this section, we explore the snap-buckling responses of layered architected materials, which transition efficiently between stable states through elastic deformation and dissipate mechanical energy without permanent damage. As illustrated in Fig. 2A, this behavior makes them well suited for applications such as vibration damping in isolators and soft wearables, providing protection for sensitive components and shielding patients from excessive forces. To unlock their potential in these applications, we use the proposed inverse design framework to program a family of snap-buckling behaviors and validate the performance experimentally.

Architected material with $N \times 1$ array

We first architect snap buckling on an $N \times 1$ array of layered unit cells, where periodic boundary conditions and design symmetry are applied along the x axis, as shown in Fig. 2C. We showcase the capability of the inverse design framework to precisely program snapping-type stress-strain responses by adjusting control targets with a tensile loading strain up to 0.4. We obtain three $N \times 1$ architected material designs (labeled as BN1-1, BN1-2, and BN1-3) that exhibit snap buckling with various initial stiffness and peak stress levels. Figure 2B shows the synergetic interaction between the red and blue layers in design BN1-3. The red and blue layers collectively ensure connectivity within the architected material. In addition, the blue layers support the red layer through anchored rigid pins to facilitate snapping responses. While the other two designs harness similar interactions, they feature unique soft material geometries and pin interconnection distribution that are crucial for achieving the

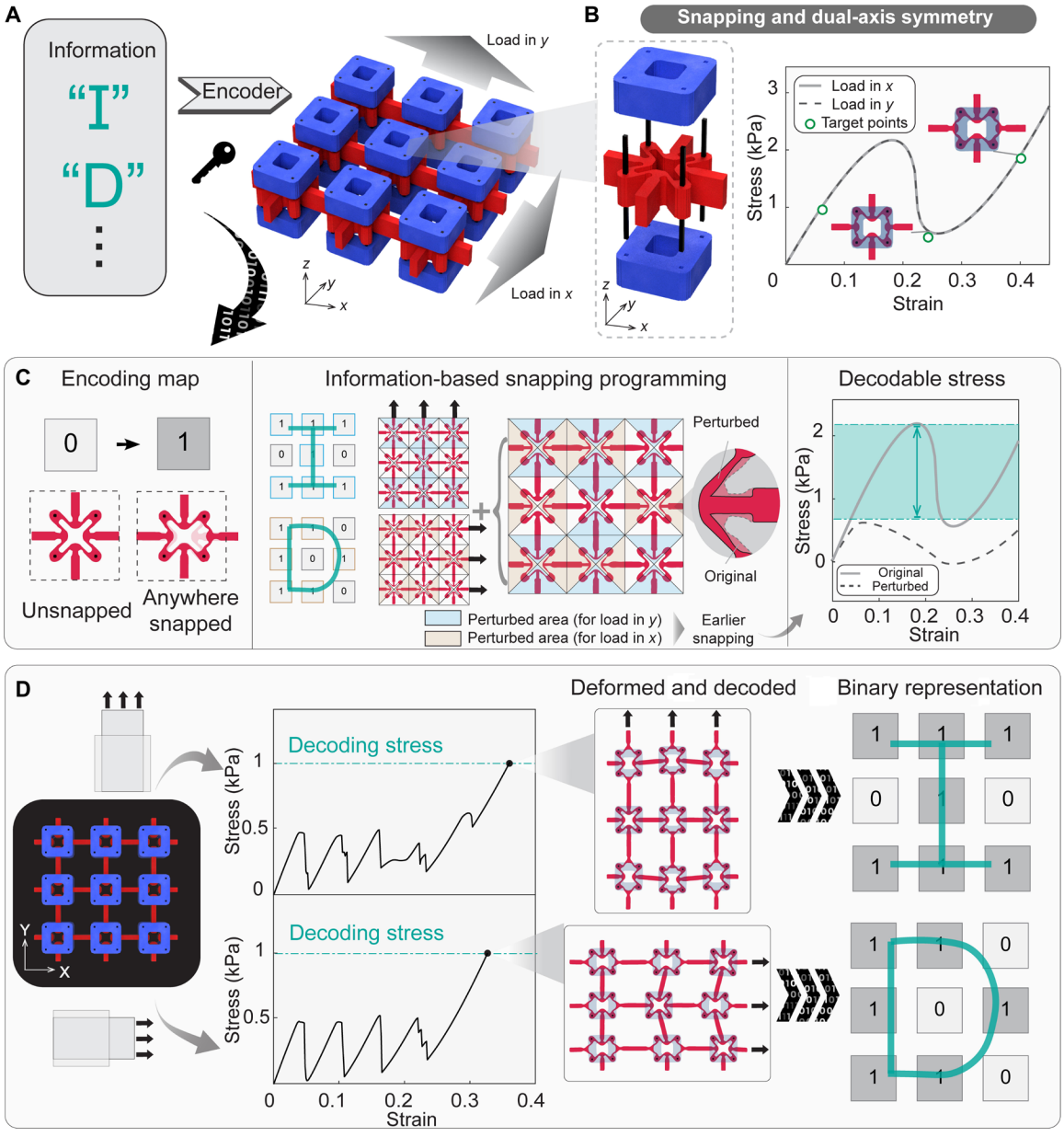

Fig. 5. Information encoding in layered nonlinear architected materials with snapping responses. (**A**) The information (I and D) to be encoded. (**B**) Designing an optimized unit cell with dual-axis symmetry that exhibits consistent snapping responses when loaded in both in-plane directions. (**C**) Encoding process. (**D**) Decoding process. See movie S2 for a demonstration of information encoding.

associated target nonlinear responses. We emphasize that the unique layer interaction mechanisms of these designs stem from the optimization-driven inverse design framework, where the distributions of the red layer, blue layer, and rigid pins are simultaneously optimized to accurately achieve the prescribed targets.

Transitioning to Fig. 2D, we conduct a comparative analysis of the responses in 3×1, 5×1, and 9×1 arrays of architected materials for design BN1-3. We introduce small perturbations in the member sizes to account for the inevitable fabrication inaccuracies encountered in practical applications. Increasing the number of unit cells in the assembly results in the following interesting observations: (i) The stress-strain curves exhibit additional peaks and valleys in the snap-through region of the original periodic unit response; (ii) despite having additional peaks and valleys, the initial and final stiffness values align with those of the periodic unit; and (iii) while the assembly response with many units no longer satisfy both peak and valley stress targets simultaneously, the peak stress level remains the same as that of the periodic unit (and target peak stress) during loading, and the valley stress coincides with that of the periodic unit (and target valley stress) during unloading. Furthermore, the interactions among local unit cells give rise to the intriguing multistage snap-back phenomenon.

Subsequently, we fabricate and experimentally test a 3×1 array of the layered architected material for design BN1-3 (unit size is 60 mm). Figure 2E illustrates the experimental setup, where the

sample is clamped at both ends in a loading machine with one end undergoing upward stretching. As anticipated from Fig. 2D, the experiment demonstrates a sequential and snap-back buckling response, progressing from the top unit cell to the bottom unit cell. Our FEA simulations, which include random size variations in the unit cell members to account for potential fabrication inaccuracies, show strong agreement with the stress-strain relation of the experimental results. This experiment validates the effective translation of our numerical design into physical prototypes, highlighting the capability of our inversely designed layered material to realize highly nonlinear snap-buckling responses.

The layered snapping architected material shows potential as a wearable device to aid recovery of joint mobility after injury or disease, as shown in Fig. 2F. This wearable offers several key benefits: (a) It is mainly made from soft materials for biomedical compatibility and comfort, reducing fatigue and reinjury risk, and (b) the snapping behavior aligns with joint rotation, providing intuitive tactile feedback during recovery. In addition, programmable stress support enables patient- and joint-specific customization, promoting healing by encouraging tissue adaptation (*39*). Unlike traditional woven support materials, this layered design allows precise control over stress-strain response, adaptable to various injury scenarios. To illustrate this application, we scale down design BN1-3 (unit size is 45 mm) to fit a knee joint. Anchored above and below the knee, the wearable snaps at specific bending angles, generating tactile feedback through vibration that helps patients monitor joint movement. As joint rotation increases, the number of snapped units also increases. While out-of-plane forces from joint contact are a potential area for future study, this demonstration indicates the layered material's promise in biomedical wearables for joint recovery.

Architected material with $N \times N$ array

Next, we architect snap buckling on an $N \times N$ array of layered materials. As shown in Fig. 3A, the design domain is subjected to periodic boundary conditions along the x and y axes with a symmetry constraint applied relative to the x axis. As shown in Fig. 3A, leveraging the inverse design framework, we produce three distinct designs (labeled as design BNN-1 to design BNN-3), demonstrating precise alignment with predefined targets with distinct valley stresses.

Found by the design framework, the architected materials in the $N \times N$ array exhibit snap buckling resulting from complex layer and unit interactions. In addition to the layer interaction found in $N \times 1$ array, i.e., blue layers providing lateral support to the red layer, each unit cell also interacts with its neighboring unit cells to obtain support within the $N \times N$ array. These supports facilitate the snap buckling phenomenon in the red layer. While the three obtained designs in Fig. 3A exhibit similar snapping mechanisms, variations in the soft material and pin distributions result in different snapping responses with distinct valley stresses. Notably, unlike design BNN-1, designs BNN-2 and BNN-3 exhibit stress valleys below zero, indicating a nonmonotonic stored energy profile with secondary energy density valleys. These secondary energy density valleys imply the appearance of bistability, which is a special case of snap buckling with interesting applications, such as microelectromechanical systems and actuators (*40*–*42*).

In Fig. 3B, we present the experimental validation for a 3×3 array prototype of design BNN-2. In contrast to the $N \times 1$ array, the edges of the $N \times N$ array are not mechanically free due to the periodicity in both in-plane directions. To realize this boundary condition approximately in the experiment, we use rollers on the nonloading sides of the 3×3 sample. The sample is clamped at both ends on a loading machine, with one end undergoing upward displacement. From the testing result, we observe a multistage buckling phenomenon progressing from the top to the bottom rows, emerging from the complex interactions between heterogeneous local architectures. Minor oscillations in the stress-strain curve are observed because of unavoidable roller friction. The measured stress-strain curve exhibits strong alignment with the FEA simulations with randomly perturbed member sizes. The experimental findings validate the physical realization of snap buckling responses in the architected layered nonlinear materials with $N \times N$ array.

Moreover, we conduct loading-unloading simulations and experiments for design BNN-2 to demonstrate its potential application in energy dissipation. As illustrated in Fig. 3C, both computational and experimental findings reveal energy dissipation during the multistage snap-back buckling under displacement loading. We note that short stress plateaus occur during the stress drop stages of the experiment, resulting from unsynchronized snapping among different units in the same row (see movie S1) due to sample imperfections. Despite these short plateau regions, the overall stress-strain relationship trend closely aligns with the simulation results. Here, each snap buckling indicates a rapid material response (i.e., rapid snap movement of the buckling members) that converts the stored elastic energy into kinetic energy and subsequently dissipates it by the material damping. This proof-of-concept capability for energy dissipation by the architected layered material holds great promise for applications related to vibration isolation and tremor suppression, as illustrated in Fig. 2A.

Architecting single and multistage plateau responses

In this section, we focus on developing layered nonlinear materials with programmable single- and multistage plateau responses. As shown in Fig. 4A, these responses enable the transfer of external energy into stored energy with customizable force plateaus. This feature is particularly advantageous for wearable devices and energy-absorbing systems. For instance, fall protection belts can use these materials to absorb kinematic energy and reduce impact forces, while car bumpers with multistage plateau responses can enhance pedestrian safety using lower plateau levels to absorb initial impact forces and higher levels for added resistance during severe collisions.

For programming single plateau responses, we set five target points to define various long plateau responses from a uniaxial tensile strain of 0.08 to 0.35. As shown in Fig. 4B, our inverse design framework effectively produces $N \times N$ array layered architected materials with precisely controlled plateau stress levels of 2.5 and 1 kPa, labeled as design PNN-1 and PNN-2, respectively. By adjusting the periodicity to apply only along the x axis, we generate $N \times 1$ array layered architected materials (labeled as PN1-1 and PN1-2), precisely achieving stress levels of 2 and 1 kPa, respectively.

Experimental tests are conducted to validate the plateau responses on designs PNN-1 and PN1-1 (with $N = 3$), shown in Fig. 4 (B and C), respectively. We observe that the measured stress-strain relations of both 3×3 and 3×1 samples align closely with the FEA results (considering member size perturbation). Here, the wavy pattern in the experimental results for assembled unit cells is primarily due to fabrication errors and other perturbation factors (such as gravity). The wavy pattern in the perturbed FEA simulations is caused by the

randomly perturbed member sizes. These perturbations cause the softening behavior of each unit to occur asynchronously, leading to sequential stress release and resulting in the observed wavy pattern. For the 3 × 3 sample in Fig. 4B, discrepancies arise after a loading strain of 0.2 due to roller-induced friction. We observe minor oscillations in the stress-strain curve, consistent with the nonsmooth sliding of the sample on the rollers (see movie S5), indicating that the primary cause is friction-induced vibrations. Both samples fail at approximately 0.32 loading strain due to the relatively low inherent fracture resistance of the used soft material. In addition, the discrepancy between the target plateau behaviors with the experimental and perturbed FEA results of the assembled structures is also caused by the small number of unit cells in the assembly. As we increase the number of unit cells, the assembled structure can gradually resemble the unit cell target behavior. In Fig. 4B, we present the simulation result for design PNN-1 assembled in a 10 × 10 array. Compared to the 3 × 3 assembly, the 10 × 10 assembly shows a closer alignment with the unit cell simulation and original target points, effectively capturing the optimized plateau-like behavior. This improved agreement is due to the separation of length scales achieved in the larger assembly.

Moreover, the developed inverse design framework can also be adjusted to produce multistage plateau responses through two different approaches, as shown in Fig. 4 (D and E). The first approach conducts optimization toward dual-plateau targets. The architected unit cell incorporates two distinct sets of softening-enabling structural members, each set facilitating a separate softening response that results in different plateau stages. During uniaxial stretching, the right pair of members undergoes softening at approximately 0.2 strain, followed by the left pair softening at a strain level near 0.5. This approach offers effective control over the multiple plateau stress levels due to direct optimization, although it may result in less smooth plateau transitions due to the limited design space in a square layered unit cell.

To expand the design space and achieve finer control over the multistage plateau response, the second approach (Fig. 4E) assembles two different unit cells with distinct single-stage plateau stress levels in series (e.g., design PN1-1 and design PN1-2), forming a composite microstructure that exhibits smoother dual-plateau response. The unit cell with lower peak stress softens first, followed by the higher peak stress unit cell. This assembly-based design approach also allows for creating materials with more than two plateau responses by integrating additional single-stage plateau unit cells. The architected layered material with multistage plateau response can achieve adaptable energy absorption under various external force (or stress) levels (*3*).

The two-stage multiplateau response can be further improved via direct optimization in a 2 × 1 design domain (or $n \times 1$ design domain in general, with $n \geq 2$). Although this approach increases the computational cost and optimization complexity, it can expand the design space and allow more design freedom to fine-tune the two-stage plateau response to be smoother by incorporating more intricate softening or snapping mechanisms in the optimized designs.

Similar to the $N \times 1$ snap-buckling design in Fig. 2D, we also investigate the effect of increasing the number of same units in the assembly for the two multistage plateau designs in Fig. 4D (unit design repeated 10 times) and Fig. 4E (each type of unit repeated 5 times). For both cases, increasing the number of units results in multiple small snapping near the target plateau stress levels and makes the responses closer to two distinct plateau stages.

Encoding information using architected dual-axis snapping

In this section, our objective shifts to information encoding on mechanical architected materials. Inspired by the multisnapping phenomenon observed in the previous sections, we can manipulate the snapping sequence and encode multiple pieces of information into the layered nonlinear architected materials. Specifically, as shown in Fig. 5A, we integrate letter shapes such as "I" and "D" into a single $N \times N$ array with snapping responses.

Within the design setup of the $N \times N$ array layered architected materials, we apply design symmetry along the *x*, *y*, and 45° axes to ensure consistent responses under loading in both *x* and *y* directions. We optimize both the material distribution within soft layers and the distribution of rigid pins to achieve the prescribed targets that define a snapping response. The optimized design, as shown in Fig. 5B, successfully achieves dual-axis snapping responses when loaded separately in both *x* and *y* directions.

In Fig. 5C, we illustrate the process of encoding information in the optimized 3 × 3 array architected materials. Here, we treat the material array as a pixelated domain and define the unit-cell level snapping as a transition from binary 0 to 1 within the associated pixel. Next, we use our understanding of the multisnapping phenomenon and intentionally perturb each unit cell to encode information. In this example, by strategically perturbing the in-plane member sizes of these unit cells, we orchestrate a snapping sequence where certain units snap earlier at a snapping peak stress lower than others. Under mechanical loading, these perturbed unit cells would snap, whereas others remain unsnapped, correlating with the binary representation on the pixelated domain to store information. Notably, because of the symmetric nature of the optimized design and independent snapping members along both *x* and *y* directions, we gain the ability to manipulate the snapping sequence and encode different information into a single 3 × 3 architected material. Moreover, it is crucial to determine the decodable loading stress, where we can pause and analyze the snapping response to decode the information. This decodable stress typically falls within the range from the peak stress of the original snapping to the peak stress of the perturbed snapping. With these considerations, pixelated information can be encoded into the $N \times N$ domain by loading the material array to the decoding stress level in both *x* and *y* directions.

To decode the information, we simply load the architected material in *x* and *y* directions to the decodable stress and analyze the resulting snapping responses for the deformed configurations. As a demonstration, the encoded 3 × 3 array shown in Fig. 5D is loaded in the *y* and *x* directions, respectively. At a loading stress level of 1 kPa, we pause and analyze the deformed shapes. By translating the snapping response into a binary representation, where 0 signifies unsnapped and 1 signifies snapped, the shapes of I and D can be unveiled. More complex information can be encoded with an increase in the number of unit cells, effectively enhancing the resolution of the pixelated domain. In addition, further adjustment of member sizes and snapping stress for each unit can also manipulate the snapping sequence with more precision, which can be used to encode the writing or drawing path of shapes into the layered architected materials.

DISCUSSION

This study proposes a strategy to create bioinspired layered architected materials to achieve extreme nonlinear responses. An inverse design paradigm is created to simultaneously optimize the local microstructure within each layer and the position of rigid pins interconnecting different layers. The synergistic interactions among different layers collectively achieve unprecedented programmability over the desired extreme nonlinear responses. The unique multilayer interaction of the layered architected material enhances the design flexibility, enabling responses that are difficult, if at all possible, to achieve with single-layer material architecture (see the Supplementary Materials for a comparison study). We conduct rigorous numerical and experimental investigations to confirm the multistage snap buckling and plateau responses, demonstrating their potential applications in energy dissipation and absorption, wearable devices, and information encoding. Leveraging the feature of multistage snap buckling, we manipulate the snapping sequence and effectively encode and store information within the architected material. With the rapid advancement of architected mechanical materials, we present a pathway to engineer future programmable materials, characterized by their layered architecture and remarkable ability to achieve precise and extreme nonlinear responses.

We discuss the multistage snap buckling observed in this study. The snapping behavior is sensitive to perturbations, such as gravity and fabrication errors, which can lead to unsynchronized snapping for an assembly of the same unit cell. The sequence of snapping depends on the type and application of these perturbations. For instance, when gravity acts downward, the top unit in a stack bears the weight of the units below, resulting in greater loading and making it more prone to snapping (see the Supplementary Materials). As the top unit snaps, the load shifts to the next unit, and this continues downward. Given insignificant fabrication errors, the snapping sequence consistently occurs top-to-bottom throughout the paper. This phenomenon can be leveraged for applications such as the information encoding shown in Fig. 5, where perturbing unit cell sizes controls the snapping sequence to encode information. Furthermore, an intriguing direction for future work is the strategical assembly of unit cell designs with diverse nonlinear behaviors to enable more complex and controllable multistage snap buckling.

Here, we also discuss the potential advancements for transitioning to real-world applications of our proposed layered architected materials. Scalability is a critical aspect for realizing viable products. We highlight that the developed inverse design paradigm offers scale-independent programmability for extreme nonlinearity. Using a hybrid fabrication technique, we demonstrate centimeter-scale prototypes. Fabricating products at millimeter scale or smaller, however, presents challenges, especially for intricate, optimized designs that may exceed the mold-making capabilities of Fused Deposition Modelling (FDM) 3D printing used in this study. Alternative approaches, such as stereolithography three-dimensional (3D) printing (*43*), electrical discharge machining (*44*), and SU-8 mold fabrication (*45*), can enable mold production at millimeter- to micrometer-level scales. In addition, direct 3D printing of soft materials such as thermoplastic polyurethane (*46*) is a promising solution. As scale decreases, bonding strength may be compromised because of reduced bonding areas; however, surface treatments (*47*, *48*) can enhance adhesion, thus improving bonding reliability and supporting the structural integrity of assembled architected materials.

Another important aspect is the stability and durability of the layered architected materials. We acknowledge that our current fabrication approach presents challenges in the following areas: The soft material, polydimethylsiloxane (PDMS) (Sylgard-184), has limited fracture resistance and may fail under large strains, and the adhesive, cyanoacrylate (super glue), bonding the soft material to the rigid pins, can degrade over extended loading and unloading cycles. However, these issues can be addressed through several strategies. Toughened silicone materials, such as Elastosil-M4630 and M4130 (*49*), offer improved long-term stability and durability due to their high elongation and tear resistance. In addition, incorporating manufacturing constraints, such as maximum stress constraints (*50*), reduces stress concentrations and enhances fracture resistance (*51*), improving long-term viability. In terms of the material bonding, surface treatments (*47*, *48*) can substantially enhance the bonding strength between the soft material and the rigid pins, thereby improving the overall stability and durability of the layered architected materials.

Furthermore, we note that the proof-of-concept demonstration of snapping-based information encoding can be extended to large-scale assemblies of layered architected unit cells to represent high-resolution pixelated domains, enabling the encoding of more complex information in practical applications. Full FEA-based analysis of large-scale assemblies could be computationally intensive, and a simplified spring system might offer a potential alternative approach (*6*). A comprehensive investigation of the encoding capability of the layered materials for more complex information warrants an interesting future study. Ensuring reliability in large-scale assemblies is also an important future direction. Encoding accuracy can be influenced by fabrication defects and uncertainties under loading conditions, which may result in snapping and decoding errors. Optimization techniques accounting for manufacturing errors and load uncertainty can potentially mitigate the impact of these uncertainties (*52*, *53*). Exploring experimental strategies to address these challenges, such as reducing loading sensitivity and boundary effects through carefully designed boundary conditions and enhancing fabrication accuracy, also offers valuable contributions for transitioning the information encoding concept toward future real-world applications.

MATERIALS AND METHODS

Material characterization

The mechanical properties of the used soft material (PDMS) with a base-to-agent ratio of 10:1 are characterized by fitting the parameters in the constitutive model to the stress-strain relationships obtained from testing dog-bone specimens in tension and cylinder specimens in compression. See the Supplementary Materials for details.

Fabrication and experimental setup

The specimens are fabricated through a hybrid 3D printing and mold casting approach. Specifically, 3D printers are used to produce water-soluble molds (made of polyvinyl alcohol) for casting soft PDMS materials with optimized geometries. Carbon fibers with much higher stiffness are used to pin the soft material layers and bonded with glue. The loading process is carried out using a uniaxial loading machine on the layered material with a displacement rate of 5 mm/min. For more information, refer to the Supplementary Materials.

Finite element analysis

To predict the mechanical response of the layered architected materials, we use FEA to conduct numerical simulations. We model the soft elastomer layers using 2D elements under the plane stress assumption and the rigid pins using 3D elements. Further details are provided in the Supplementary Materials.

Inverse-design optimization algorithm

The inverse-design optimization algorithm is developed to generate the designs in this study. It simultaneously optimizes the geometry of the soft material and the distribution of the rigid pins. The optimization process formulates an inverse problem by minimizing the error between the FEA simulation and the prescribed target responses at multiple control points. Our inverse-design optimization algorithm enables scale-independent programmability of stress-strain nonlinearity by automatically generating designs for arbitrary design domains, normalizing size within the controlled stress-strain response, and accurately accounting for the experimentally characterized base material's nonlinear properties. Further details can be found in the Supplementary Materials.

Supplementary Materials

The PDF file includes:

Supplementary Text
Figs. S1 to S5
Legends for movies S1 to S5
References

Other Supplementary Material for this manuscript includes the following:

Movies S1 to S5

REFERENCES AND NOTES

1. P. Jiao, J. Mueller, J. R. Raney, X. Zheng, A. H. Alavi, Mechanical metamaterials and beyond. *Nat. Commun.* **14**, 6004 (2023).
2. N. San Ha, G. Lu, A review of recent research on bio-inspired structures and materials for energy absorption applications. *Compos. Part B Eng.* **181**, 107496 (2020).
3. Q. Zeng, S. Duan, Z. Zhao, P. Wang, H. Lei, Inverse design of energy-absorbing metamaterials by topology optimization. *Adv. Sci.* **10**, e2204977 (2023).
4. J. Mo, R. Priefer, Medical devices for tremor suppression: Current status and future directions. *Biosensors* **11**, 99 (2021).
5. Z. Meng, H. Yan, M. Liu, W. Qin, G. M. Genin, C. Q. Chen, Encoding and storage of information in mechanical metamaterials. *Adv. Sci.* **10**, e2301581 (2023).
6. W. Li, F. Wang, O. Sigmund, X. S. Zhang, Digital synthesis of free-form multimaterial structures for realization of arbitrary programmed mechanical responses. *Proc. Natl. Acad. Sci. U.S.A.* **119**, e2120563119 (2022).
7. H. Ma, K. Wang, H. Zhao, Y. Hong, Y. Zhou, J. Xue, Q. Li, G. Wang, B. Yan, Energy dissipation in multistable auxetic mechanical metamaterials. *Compos. Struct.* **304**, 116410 (2023).
8. K. W. Hector, G. Jarrold, Y. Cho, D. Restrepo, N. Mankame, P. D. Zavattieri, Energy dissipating architected materials with transversely curved tapes and independently tunable properties. *Extreme Mech. Lett.* **58**, 101946 (2023).
9. A. Alomarah, Y. Yuan, D. Ruan, A bio-inspired auxetic metamaterial with two plateau regimes: Compressive properties and energy absorption. *Thin-Walled Struct.* **192**, 111175 (2023).
10. X. Xin, L. Liu, Y. Liu, J. Leng, 4D pixel mechanical metamaterials with programmable and reconfigurable properties. *Adv. Funct. Mater.* **32**, 2107795 (2022).
11. L. Y. W. Loh, U. Gupta, Y. Wang, C. C. Foo, J. Zhu, W. F. Lu, 3D printed metamaterial capacitive sensing array for universal jamming gripper and human joint wearables. *Adv. Eng. Mater.* **23**, 2001082 (2021).
12. D. Yigci, A. Ahmadpour, S. Tasoglu, AI-based metamaterial design for wearables. *Adv. Sens. Res.* **3**, 2300109 (2024).
13. Y. Wang, L. Li, D. Hofmann, J. E. Andrade, C. Daraio, Structured fabrics with tunable mechanical properties. *Nature* **596**, 238–243 (2021).
14. F. Wang, O. Sigmund, J. S. Jensen, Design of materials with prescribed nonlinear properties. *J. Mech. Phys. Solids* **69**, 156–174 (2014).
15. J.-H. Bastek, D. M. Kochmann, Inverse-design of nonlinear mechanical metamaterials via video denoising diffusion models. *Nat. Mach. Intel.* **5**, 1466–1475 (2023).
16. W. Li, F. Wang, O. Sigmund, X. S. Zhang, Design of composite structures with programmable elastic responses under finite deformations. *J. Mech. Phys. Solids* **151**, 104356 (2021).
17. R. Rabiei, S. Bekah, F. Barthelat, Nacre from mollusk shells: Inspiration for high-performance nanocomposites. Natural Polymers (Royal Society of Chemistry, 2012), pp. 113–149; https://doi.org/10.1039/9781849735315-00113.
18. M. A. Monn, K. Vijaykumar, S. Kochiyama, H. Kesari, Lamellar architectures in stiff biomaterials may not always be templates for enhancing toughness in composites. *Nat. Commun.* **11**, 373 (2020).
19. O. Sigmund, Tailoring materials with prescribed elastic properties. *Mech. Mater.* **20**, 351–368 (1995).
20. G. Nika, A. Constantinescu, Design of multi-layer materials using inverse homogenization and a level set method. *Comput. Methods Appl. Mech. Eng.* **346**, 388–409 (2019).
21. J. Sim, S. Wu, J. Dai, R. R. Zhao, Magneto-mechanical bilayer metamaterial with global area-preserving density tunability for acoustic wave regulation. *Adv. Mater.* **35**, e2303541 (2023).
22. R. Guseinov, C. McMahan, J. Pérez, C. Daraio, B. Bickel, Programming temporal morphing of self-actuated shells. *Nat. Commun.* **11**, 237 (2020).
23. Y. Liu, Y. Wang, H. Ren, Z. Meng, X. Chen, Z. Li, L. Wang, W. Chen, Y. Wang, J. du, Ultrastiff metamaterials generated through a multilayer strategy and topology optimization. *Nat. Commun.* **15**, 2948 (2024).
24. O. Sigmund, Materials with prescribed constitutive parameters: An inverse homogenization problem. *Int. J. Solids Struct.* **31**, 2313–2329 (1994).
25. A. Clausen, F. Wang, J. S. Jensen, O. Sigmund, J. A. Lewis, Topology optimized architectures with programmable Poisson's ratio over large deformations. *Adv. Mater.* **27**, 5523–5527 (2015).
26. Y. Mao, Q. He, X. Zhao, Designing complex architectured materials with generative adversarial networks. *Sci. Adv.* **6**, 10.1126/sciadv.aaz4169 (2020).
27. B. Deng, A. Zareei, X. Ding, J. C. Weaver, C. H. Rycroft, K. Bertoldi, Inverse design of mechanical metamaterials with target nonlinear response via a neural accelerated evolution strategy. *Adv. Mater.* **34**, e2206238 (2022).
28. T. Zhou, X. Wan, D. Z. Huang, Z. Li, Z. Peng, A. Anandkumar, J. F. Brady, P. W. Sternberg, C. Daraio, AI-aided geometric design of anti-infection catheters. *Sci. Adv.* **10**, eadj1741 (2024).
29. M. P. Bendsoe, O. Sigmund, *Topology Optimization: Theory, Methods, and Applications* (Springer Science & Business Media, 2013).
30. C. Wang, Z. Zhao, M. Zhou, O. Sigmund, X. S. Zhang, A comprehensive review of educational articles on structural and multidisciplinary optimization. *Struct. Multidiscip. Optim.* **64**, 2827–2880 (2021).
31. D. Thillaithevan, R. Murphy, R. Hewson, M. Santer, Inverse design of periodic microstructures with targeted nonlinear mechanical behaviour. *Struct. Multidiscip. Optim.* **67**, 55 (2024).
32. C. S. Ha, D. Yao, Z. Xu, C. Liu, H. Liu, D. Elkins, M. Kile, V. Deshpande, Z. Kong, M. Bauchy, X. Zheng, Rapid inverse design of metamaterials based on prescribed mechanical behavior through machine learning. *Nat. Commun.* **14**, 5765 (2023).
33. L. Wu, D. Pasini, In situ activation of snap-through instability in multi-response metamaterials through multistable topological transformation. *Adv. Mater.* **35**, e2301109 (2023).
34. J.-H. Bastek, D. M. Kochmann, Inverse design of nonlinear mechanical metamaterials via video denoising diffusion models. *Nat. Mach. Intell.* **5**, 1466–1475 (2023).
35. R. V. Woldseth, N. Aage, J. A. Bærentzen, O. Sigmund, On the use of artificial neural networks in topology optimisation. *Struct. Multidiscip. Optim.* **65**, 294 (2022).
36. N. Hu, R. Burgueño, Buckling-induced smart applications: Recent advances and trends. *Smart Mater. Struct.* **24**, 063001 (2015).
37. M. Sun, X. Hu, L. Tian, X. Yang, L. Min, Auxetic biomedical metamaterials for orthopedic surgery applications: A comprehensive review. *Orthop. Surg.* **16**, 1801–1815 (2024).
38. K. Svanberg, The method of moving asymptotes–a new method for structural optimization. *Int. J. Numer. Methods Eng.* **24**, 359–373 (1987).
39. L. M. Cyr, R. G. Ross, How controlled stress affects healing tissues. *J. Hand Ther.* **11**, 125–130 (1998).
40. Y. Cao, M. Derakhshani, Y. Fang, G. Huang, C. Cao, Bistable structures for advanced functional systems. *Adv. Funct. Mater.* **31**, 2106231 (2021).
41. K. Liang, Y. Wang, Y. Luo, A. Takezawa, X. Zhang, Z. Kang, Programmable and multistable metamaterials made of precisely tailored bistable cells. *Mater. Des.* **227**, 111810 (2023).
42. Z. Zhao, X. S. Zhang, Encoding reprogrammable properties into magneto-mechanical materials via topology optimization. *npj Comput. Mater.* **9**, 57 (2023).
43. O. Aydin, K. Hirashima, M. T. A. Saif, Incorporating geometric nonlinearity in theoretical modeling of muscle-powered soft robotic bio-actuators. *J. Appl. Mech.* **91**, 011008 (2024).
44. K. Ho, S. Newman, State of the art electrical discharge machining (EDM). *Int. J. Mach. Tool Manuf.* **43**, 1287–1300 (2003).

45. A. del Campo, C. Greiner, SU-8: A photoresist for high-aspect-ratio and 3D submicron lithography. *J. Micromech. Microeng.* **17**, R81–R95 (2007).
46. S. M. Desai, R. Y. Sonawane, A. P. More, Thermoplastic polyurethane for three-dimensional printing applications: A review. *Polym. Adv. Technol.* **34**, 2061–2082 (2023).
47. A. Borók, K. Laboda, A. Bonyár, PDMS bonding technologies for microfluidic applications: A review. *Biosensors* **11**, 292 (2021).
48. V. Sunkara, D.-K. Park, Y.-K. Cho, Versatile method for bonding hard and soft materials. *RSC Adv.* **2**, 9066–9070 (2012).
49. S. Park, K. Mondal, R. M. Treadway III, V. Kumar, S. Ma, J. D. Holbery, M. D. Dickey, Silicones for stretchable and durable soft devices: Beyond Sylgard-184. *ACS Appl. Mater. Interfaces* **10**, 11261–11268 (2018).
50. M. Bruggi, On an alternative approach to stress constraints relaxation in topology optimization. *Struct. Multidiscip. Optim.* **36**, 125–141 (2008).
51. J. Yvonnet, D. Da, Topology optimization to fracture resistance: A review and recent developments. *Arch. Comput. Methods Eng.* **31**, 2295–2315 (2024).
52. P. D. Dunning, H. A. Kim, G. Mullineux, Introducing loading uncertainty in topology optimization. *AIAA J.* **49**, 760–768 (2011).
53. M. Schevenels, B. S. Lazarov, O. Sigmund, Robust topology optimization accounting for spatially varying manufacturing errors. *Comput. Methods Appl. Mech. Eng.* **200**, 3613–3627 (2011).
54. O. Lopez-Pamies, A new I_1-based hyperelastic model for rubber elastic materials. *CR Mecanique* **338**, 3–11 (2010).
55. T. Belytschko, W. K. Liu, B. Moran, K. Elkhodary, *Nonlinear Finite Elements for Continua and Structures* (John Wiley & Sons, 2014).
56. L. Armijo, Minimization of functions having Lipschitz continuous first partial derivatives. *Pacific J. Math.* **16**, 1–3 (1966).
57. X. Zhang, A. S. Ramos, G. H. Paulino, Material nonlinear topology optimization using the ground structure method with a discrete filtering scheme. *Struct. Multidiscipl. Opti.* **55**, 2045–2072 (2017).
58. T. J. Hughes, M. Cohen, M. Haroun, Reduced and selective integration techniques in the finite element analysis of plates. *Nucl. Eng. Des.* **46**, 203–222 (1978).
59. M. P. Bendsoe, O. Sigmund, *Topology Optimization: Theory, Methods, and Applications* (Springer Science & Business Media, 2003).
60. F. Wang, B. S. Lazarov, O. Sigmund, On projection methods, convergence and robust formulations in topology optimization. *Struct. Multidiscip. Optim.* **43**, 767–784 (2011).
61. Z. Zhao, X. S. Zhang, Topology optimization of hard-magnetic soft materials. *J. Mech. Phys. Solids* **158**, 104628 (2022).
62. M. Schevenels, O. Sigmund, On the implementation and effectiveness of morphological close-open and open-close filters for topology optimization. *Struct. Multidiscip. Optim.* **54**, 15–21 (2016).
63. F. Wang, B. S. Lazarov, O. Sigmund, J. S. Jensen, Interpolation scheme for fictitious domain techniques and topology optimization of finite strain elastic problems. *Comput. Methods Appl. Mech. Eng.* **276**, 453–472 (2014).
64. P. Duysinx, M. P. Bendsøe, Topology optimization of continuum structures with local stress constraints. *Int. J. Numer. Methods Eng.* **43**, 1453–1478 (1998).

Acknowledgments

Funding: This material is based on work supported by the Air Force Office of Scientific Research under award number FA9550-23-1-0297. In addition, X.S.Z. acknowledges the support from US National Science Foundation (NSF) CAREER award CMMI-2047692 and NSF award CMMI-2245251. O.S. was supported by the Villum Investigator Project AMSTRAD (VIL54487) from Villum Fonden.
Author contributions: Conceptualization: O.S. and X.S.Z. Methodology: Z.Z., R.D.K., O.S., and X.S.Z. Software: Z.Z. and R.D.K., Investigation: Z.Z., R.D.K., O.S., and X.S.Z. Visualization: Z.Z., R.D.K., and X.S.Z., Supervision: O.S. and X.S.Z. Writing—original draft: Z.Z., R.D.K., and X.S.Z. Writing—review and editing: Z.Z., R.D.K., O.S., and X.S.Z. **Competing interests:** The authors declare that they have no competing interests. **Data and materials availability:** All data needed to evaluate the conclusions in the paper are available in the main text and/or the Supplementary Materials.

Submitted 18 July 2024
Accepted 15 April 2025
Published 16 May 2025
10.1126/sciadv.adr6925